Testing fast photochemical theory during TRACE-P based on measurements of OH, HO2 , and CH2O

Testing fast photochemical theory during TRACE-P based on measurements of OH, HO_2, and CH_2O

Jennifer R. Olson,[1] J. H. Crawford,[1] G. Chen,[1] A. Fried,[2] M. J. Evans,[3] C. E. Jordan,[1] S. T. Sandholm,[4] D. D. Davis,[4] B. E. Anderson,[1] M. A. Avery,[1] J. D. Barrick,[1] D. R. Blake,[5] W. H. Brune,[6] F. L. Eisele,[2] F. Flocke,[2] H. Harder,[6,7] D. J. Jacob,[3] Y. Kondo,[8] B. L. Lefer,[2] M. Martinez[6,7] R. L. Mauldin,[2] G. W. Sachse,[1] R. E. Shetter,[2] H. B. Singh,[9] R. W. Talbot,[10] and D. Tan[4]

Received 23 October 2003; revised 22 March 2004; accepted 1 April 2004; published 22 June 2004.

[1] Measurements of several short-lived photochemical species (e.g., OH, HO_2, and CH_2O) were obtained from the DC-8 and P3-B aircraft during the NASA Transport and Chemical Evolution over the Pacific (TRACE-P) campaign. To assess fast photochemical theory over the east Asian coast and western Pacific, these measurements are compared to predictions using a photochemical time-dependent box model constrained by coincident measurements of long-lived tracers and physical parameters. Both OH and HO_2 are generally overpredicted by the model throughout the troposphere, which is a different result from previous field campaigns. The calculated-to-observed ratio of OH shows an altitude trend, with OH overpredicted by 80% in the upper troposphere and by 40–60% in the middle troposphere. Boundary layer and lower tropospheric OH ratios decrease from middle tropospheric values to 1.07 for the DC-8 and to 0.70 for the P3-B. HO_2 measured on the DC-8 is overpredicted by a median of 23% and shows no trend in the agreement with altitude. Three subsets of data which compose 12% of the HO_2 measurements represent outliers with respect to calculated-to-observed ratios: stratospherically influenced air, upper tropospheric data with NO > 135 pptv, and data from within clouds. Pronounced underpredictions of both HO_2 and OH were found for stratospherically influenced air, which is in contrast to previous studies showing good agreement of predicted and observed HO_x in the stratosphere. Observational evidence of heterogeneous uptake of HO_2 within low and middle tropospheric clouds is presented, though there is no indication of significant HO_2 uptake within higher-altitude clouds. Model predictions of CH_2O are in good agreement with observations in the median for background concentrations, but a large scatter exists. Factors contributing to this scatter are examined, including the limited availability of some important constraining measurements, particularly CH_3OOH. Some high concentrations of CH_2O near the coast are underpredicted by the box model as a result of the inherent neglect of transport effects of CH_2O and its precursors via the steady state assumption; however, these occurrences are limited to ~1% of the data. For the vast majority of the atmosphere, transport is unimportant in the budget of CH_2O, which may be considered to be in steady state. *INDEX TERMS:* 0365 Atmospheric Composition and Structure: Troposphere—composition and chemistry; 0368 Atmospheric Composition and Structure: Troposphere—constituent transport and chemistry; *KEYWORDS:* TRACE-P, photochemistry, tropospheric chemistry

Citation: Olson, J. R., et al. (2004), Testing fast photochemical theory during TRACE-P based on measurements of OH, HO_2, and CH_2O, *J. Geophys. Res.*, *109*, D15S10, doi:10.1029/2003JD004278.

[1]Atmospheric Sciences Division, Langley Research Center, NASA, Hampton, Virginia, USA.
[2]Atmospheric Chemistry Division, National Center for Atmospheric Research, Boulder, Colorado, USA.
[3]Division of Engineering and Applied Science, Harvard University, Cambridge, Massachusetts, USA.
[4]School of Earth and Atmospheric Sciences, Georgia Institute of Technology, Atlanta, Georgia, USA.
[5]Department of Earth System Science, University of California, Irvine, California, USA.
[6]Department of Meteorology, Pennsylvania State University, University Park, Pennsylvania, USA.
[7]Now at Max Planck Institute for Chemistry, Mainz, Germany.
[8]Solar-Terrestrial Environmental Laboratory, Nagoya University, Nagoya, Japan.
[9]Earth Science Division, NASA Ames Research Center, Moffett Field, California, USA.
[10]Institute for the Study of Earth, Oceans, and Space, Climate Change Research Center, University of New Hampshire, Durham, New Hampshire, USA.

0148-0227/04/2003JD004278

1. Introduction

[2] NASA's Transport and Chemical Evolution over the Pacific (TRACE-P) field campaign was conducted along the Asian Pacific Rim and the western Pacific during February–April 2001 [*TRACE-P Science Team*, 2003]. In situ sampling of a broad suite of trace gases, aerosols, and meteorological parameters were provided from two aircraft, NASA's DC-8 and P3-B. The goals of TRACE-P were (1) to determine the composition of Asian outflow over the western Pacific in spring in order to understand and quantify the export of chemically and radiatively important gases and aerosols and their precursors from the Asian continent and (2) to determine the chemical evolution of the Asian outflow over the western Pacific in spring and to understand the ensemble of processes that control this evolution.

[3] An examination of fast photochemical cycles and their role in altering the chemical composition of Asian outflow is central to the second objective. These cycles involve short-lived chemical species that can be measured as well as theoretically predicted from in situ conditions. Test species available for examination in the TRACE-P data include the hydroxyl (OH) and hydroperoxyl (HO_2) radicals and formaldehyde (CH_2O). This paper presents results of a diurnal steady state modeling analysis of fast photochemistry using measurements during the TRACE-P campaign.

[4] The role of HO_x as central in the determination of the atmosphere's oxidative capacity has been well established. OH is pivotal to understanding photochemical ozone formation, removal of pollutant gases, and new particle formation. In the lower troposphere, the principal source of HO_x is from the reaction of the excited state $O(^1D)$ with water vapor following O_3 photolysis, and in the presence of extremely low water vapor (such as in the upper troposphere), photolysis of acetone can become the dominant source [*Singh et al.*, 1995]. Secondary production of HO_x stems from the oxidation of hydrocarbons. Though this process initially consumes OH, further reactions of products from hydrocarbon oxidation such as formaldehyde (CH_2O) can in turn produce multiple HO_2 radicals. Additionally, species such as peroxides that are typically considered to be in equilibrium with HO_x can become local sources when transport-induced nonequilibrium conditions occur, such as the convective transport of abundant peroxides from the boundary layer into the free troposphere [*Jaeglé et al.*, 1997; *Prather and Jacob*, 1997]. HO_x losses include the self-reaction of HO_2 to form H_2O_2, reaction of OH with HO_2, and reaction of OH with NO_2 to form HNO_3. Internal recycling of HO_x is largely dependent on NO and CO and is important both in the definition of the O_3-forming potential of the environment and in the efficiency of the HO_x sinks.

[5] Formaldehyde plays an important role in the cycling of HO_x, particularly as it relates to the oxidation of hydrocarbons. CH_2O is an intermediate product in the oxidation by OH of methane and other hydrocarbons; its major global source is photochemical production. In addition, CH_2O is directly emitted from industrial combustion and biomass burning, though these sources are expected to be relatively minor [*Sigsby et al.*, 1987; *Lee et al.*, 1997]. CH_2O losses include oxidation by OH and photolysis. Photolysis proceeds through two branches, one of which leads to formation of HO_x, while a secondary branch leads to stable products. Thus the photochemical cycling of CH_2O is intimately tied to both hydrocarbon degradation, which itself has considerable uncertainty, and to HO_x formation. This, along with the fact that CH_2O can be more sensitive than HO_x to changes in precursor species, makes it a particularly important test species for improving our understanding of photochemical cycling [*Crawford et al.*, 1999].

2. Model Description

[6] The analysis presented here is based on calculations from a time-dependent photochemical box model, which has been described in detail in several previous studies [e.g., *Crawford et al.*, 1999]. The approach used is diurnal steady state modeling, whereby long-lived precursor species are constrained to observations. Model-calculated species are then assumed to be at diurnal steady state, meaning that these predicted concentrations are integrated in time until their diurnal cycles no longer vary from day to day. The model chemistry includes basic HO_x-NO_x-CH_4 gas phase reactions based on the recommendations of *Atkinson et al.* [1992], *Sander et al.* [2000], and *Ravishankara et al.* [2002]. Nonmethane hydrocarbon (NMHC) chemistry is based on the condensed mechanism of *Lurmann et al.* [1986] with modifications included to address remote low-NO_x conditions and to represent explicit chemistry for acetone, propane, and benzene. Surface and heterogeneous losses for soluble species are simulated as by *Logan et al.* [1981].

[7] Photolysis rate coefficients are based on measurements. A DISORT four-stream implementation of the National Center for Atmospheric Research Tropospheric Ultraviolet-Visible (TUV) radiative transfer code is first used to calculate the diurnal variations of photolysis coefficients for clear-sky conditions. To account for local radiative conditions, these modeled clear-sky photolysis rates are then normalized throughout the day using a cloud correction factor (CCF) such that in situ spectroradiometer photolysis measurements are exactly matched at the time of the measurement [*Shetter and Müller*, 1999].

[8] Model calculations use the 1-min merged data set available on the GTE TRACE-P public data archive (http://www-gte.larc.nasa.gov). Model calculations require a minimum set of input constraints; these include observations of O_3, CO, NO, NMHC, temperature, H_2O (dew/frost point), pressure, and photolysis rates. Nonmethane hydrocarbons are constrained to observations where available (53% of the data) and are interpolated from adjacent measurements in data gaps of <5 min (37% of the data). Data gaps of >5 min were interpolated and examined subjectively for adequacy (10% of the data). Acetone and methyl ethyl ketone (MEK) are constrained to observations when data are available and are filled in the upper troposphere using an empirical relationship with CO. Missing data for methanol are filled throughout the troposphere. Model analysis is also limited to conditions with solar zenith angles <80°. There are 5167 points from the DC-8 (59% of the total) that meet the criteria for modeling, and 6621 points from the P3-B (70% of the total) are analyzed.

[9] In addition to the required constraints described above, the model constrains the following species when measurements are available: Hydrogen peroxide (H_2O_2), methyl hydrogen peroxide (CH_3OOH), nitric acid (HNO_3), and peroxy acetyl nitrate (PAN). If unavailable, these species are calculated to be in diurnal photochemical equilibrium. Impacts on model results from the limited availability of observations for these species are addressed in sections 3.2 and 4.2.2.

[10] With the exception of NO, constraining parameters are held constant throughout the diurnal cycle. Short-lived nitrogen ($NO + NO_2 + NO_3 + 2N_2O_5 + HONO + HNO_4$) is photochemically partitioned at each time step, while the total short-lived nitrogen is held constant to a value such that predicted NO matches the measurement at the time of observation.

3. Observational Data and Modeling Approach

3.1. Oxygenated Hydrocarbon Data

[11] At upper tropospheric altitudes (e.g., above 7 or 8 km), oxygenated hydrocarbons such as acetone, MEK, methanol, and ethanol can constitute an important primary source of HO_x [e.g., *Singh et al.*, 1995; *Jaeglé et al.*, 1998, 2000; *Crawford et al*, 1999]. Measurements of these oxygenates were obtained from the DC-8, which has a flight ceiling of 12 km and therefore flies within the altitudes where these species are expected to influence HO_x. The median value of acetone measurements was 565 pptv at these upper altitudes, while that for MEK was 26 pptv. The alcohols methanol and ethanol were measured at median values of 711 and 33 pptv, respectively. No measurements of oxygenates were made on board the P3-B during TRACE-P. However, the P3-B flight ceiling is 7 km, below the altitude at which oxygenates are expected to become important components of the HO_x budget.

[12] Figure 1 shows the altitude dependence of oxygenate influence on HO_x. Results are shown relative to base calculations that neglect oxygenates, illustrating the impact on HO_2 from ketones (acetone and MEK, open boxes) and the combined impact from both ketones and alcohols (solid boxes). Increases in HO_2 due to oxygenates are most significant in the upper troposphere (>11 km), with enhancements of up to 60–80%. The importance of oxygenates declines with decreasing altitudes; below 7 km, the median increase to HO_2 is <5%, and the impact on OH is <1% (not shown). From this it can be concluded that an analysis of HO_x data from the P3-B aircraft is not compromised by the absence of oxygenate data. Note that the majority of the increases due to ketones in Figure 1 are attributed to acetone; MEK has only a limited role in the HO_x increases. Figure 1 also illustrates that the impact from alcohols is significantly less than the impact from ketones.

[13] Data coverage for oxygenate measurements on the DC-8 was ~25% from 8 to 12 km, necessitating a method of estimation for points with missing values. At these altitudes, median measured CO was 117 ppbv. An empirical relationship for acetone and CO was derived from data at 8–12 km and was used to fill missing measurements for acetone as

$$\text{acetone(pptv)} = -92. + 6.27*[\text{CO(ppbv)}]. \quad (1)$$

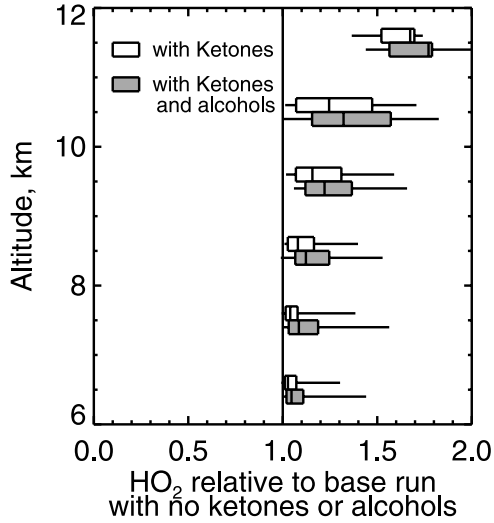

Figure 1. Impact of oxygenates on predicted HO_2. Model results for HO_2 are shown as a function of altitude and relative to a base run that neglects the impact of oxygenates. Boxes show the inner 50th percentile of the ratios, and whiskers indicate the inner 90th percentile. Median values are shown by the center lines within the boxes. The impact from ketones (acetone and methyl ethyl ketone) is shown by the open boxes, and the combined impact of ketones and alcohols (methyl and ethyl alcohol) is shown by the solid boxes.

The relation in equation (1) gives an r^2 coefficient of 0.81 for observed versus calculated acetone and is notably similar to that derived by *McKeen et al.* [1997] for data above 9 km in the western Pacific during February and March 1994 during the Pacific Exploratory Mission (PEM) West B field campaign (acetone (pptv) = −126.8 + 6.12*[CO(ppbv)]). Similarly, missing methanol values are filled on the basis of an empirical nonlinear relation to acetone derived from the TRACE-P data. MEK is assumed to equal a 5% fraction of the acetone mixing ratio, and ethanol is assumed to equal a 5% fraction of methanol.

[14] The oxidation of methanol via OH represents a small but nonnegligible source of CH_2O throughout the troposphere. Thus it is necessary to extend data filling for methanol to altitudes below 8 km, where the coverage for CH_3OH measurements on the DC-8 is 30%. Methanol was measured at these altitudes during TRACE-P at a median value of 895 pptv, and at these concentrations, the model calculations show the impact on CH_2O predictions is on the order of 10%, similar to results presented by *Frost et al.* [2002]. Missing methanol data points at these lower altitudes are therefore also filled on the basis of empirical nonlinear fits to CO derived from the TRACE-P measurements.

3.2. Peroxide Data

[15] Another source of uncertainty in model predictions of HO_x results from the limited availability of peroxide data. Measurements are available 48% of the time for H_2O_2 and 47% of the time for CH_3OOH. The median measured value of H_2O_2 in the lower troposphere (below 4 km) during TRACE-P was 635 pptv, which decreased to 165 pptv at

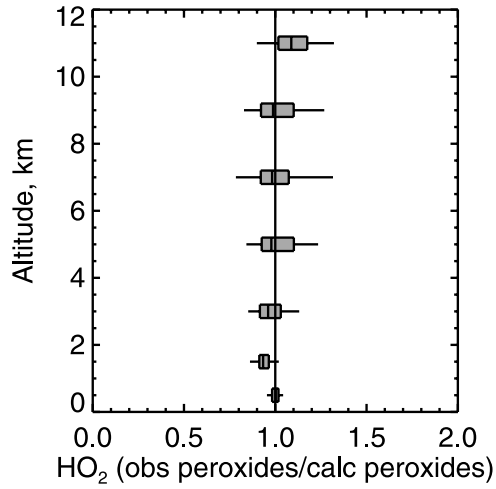

Figure 2. Impact of using observed versus calculated peroxides on predicted HO_2. See Figure 1 caption for definition of box and whiskers. Model predictions of HO_2 are shown for a simulation using observed H_2O_2 and CH_3OOH relative to a simulation where these peroxides are calculated by the model. Ratios thus indicate the incidence and impact of nonequilibrium peroxide conditions on HO_2.

altitudes >8 km. The median measurement of CH_3OOH was 215 pptv at altitudes below 4 km and was 80 pptv in the upper troposphere. For points without available measurements, concentrations are calculated by the model in photochemical diurnal steady state. Deviations from this equilibrium are expected, however, because of physical processes such as wet removal and transport influences (e.g., convective transport of peroxides into the upper troposphere). Test model simulations were conducted, calculating peroxides at points with available measurements in order to test both the ability of the model to predict peroxides and the influence of nonequilibrium peroxides on HO_x. H_2O_2 is generally overpredicted by the model by 30–40%. Prominent exceptions are for the 1–2 km layer, which showed model overpredictions of factors of 2–3 due to the model assumption limiting H_2O_2 surface deposition to a 1-km boundary layer depth and at altitudes above 10 km, which had a median model underprediction of 25%. CH_3OOH is overpredicted below 4 km by a median of 40% and is underpredicted by 40% in the upper troposphere, similar to results from previous studies [e.g., *Olson et al.*, 2001]. Despite the differences in calculated versus observed peroxides, Figure 2 shows that the ultimate impact on calculated HO_2 is minimal. The results are shown as the ratio of predicted HO_2 for model simulations using observed peroxides versus calculated peroxides; thus the ratio is a measure of the influence of nonequilibrium peroxides on HO_x during TRACE-P. While it may be argued that some increase in HO_2 (~10%) occurs above 10 km as a result of using observed peroxides, the median ratio is near 1 throughout most of the troposphere, indicating that while nonequilibrium conditions do exist for peroxides on a point-by-point basis, the overall bulk statistics for comparing measured and calculated HO_x should be relatively insensitive to the availability of peroxide observations during TRACE-P. This conclusion is also supported by the analysis by *Davis et al.* [2003].

4. Discussion of Results

4.1. HO_x

[16] Direct measurements of HO_x have been implemented from airborne platforms only since the 1990s, and results of comparison with theory have yielded inconsistencies from campaign to campaign. Measurements from the Stratospheric Tracers of Atmospheric Transport (STRAT) and Subsonic Aircraft Contrail and Cloud Effects Special Study (SUCCESS) campaigns indicated large HO_x model underpredictions in the upper troposphere by up to 50–75% [*Jaeglé et al.*, 1997; *Wennberg et al.*, 1998; *Brune et al.*, 1998]. HO_x predictions during SASS (Subsonic Assessment) Ozone and Nitrogen Oxides Experiment (SONEX) were generally good, though some trends in the agreement related to solar zenith angle and NO_x were discussed [*Jaeglé et al.*, 2000; *Brune et al.*, 1999]. In contrast, predictions of upper tropospheric HO_2 were ~10% larger than measurements during PEM-Tropics B [*Olson et al.*, 2001]. While suggestions of convective transport of peroxides and formaldehyde could explain the upper tropospheric HO_x imbalance during STRAT and SUCCESS, the lack of measurements for these precursors prevented a definitive investigation [*Jaeglé et al.*, 1997, 1998]. Evidence of significant influence of these precursors on HO_x was not found during the SONEX or PEM-Tropics B campaigns, however.

[17] Predictions of the upper tropospheric HO_2/OH ratio have likewise been inconsistent between campaigns. While this ratio was in general agreement with observations during STRAT and SONEX [*Jaeglé et al.*, 1997, 2000], it was underpredicted during SUCCESS by 30% [*Brune et al.*, 1998]. Conversely, the HO_2/OH ratio was overestimated by models in the upper troposphere during PEM-Tropics B by 30% [*Olson et al.*, 2001].

[18] Agreement of models and measurements for HO_x in the lower troposphere has been somewhat more consistent, although the quantity of the measurements is limited. Analysis of OH in the lower troposphere from the ACE-1 [*Mauldin et al.*, 1998; *Chen et al.*, 2001], PEM-Tropics A [*Mauldin et al.*, 1999] and PEM-Tropics B [*Olson et al.*, 2001] field campaigns showed modeled OH values that were typically slightly higher than measurements. The only field campaign measurements of HO_2 in the lower troposphere (PEM-Tropics B) also showed slight model overpredictions in the boundary layer and good agreement in the middle troposphere [*Olson et al.*, 2001].

4.1.1. HO_x Model-to-Observations Comparisons During TRACE-P

[19] OH measurements were made on the P3-B using a multichannel selected ion chemical ionization mass spectrometer system with a reported error of 60% [*Mauldin et al.*, 2003] and a data coverage of 75% of the modeled points. While HO_2 measurements were also obtained, using a chemical ionization mass spectrometer [*Cantrell et al.*, 2003], coverage with this technique was sparse and is not included in this analysis.

[20] On board the DC-8, OH and HO_2 measurements were obtained with the Penn State Airborne Tropospheric

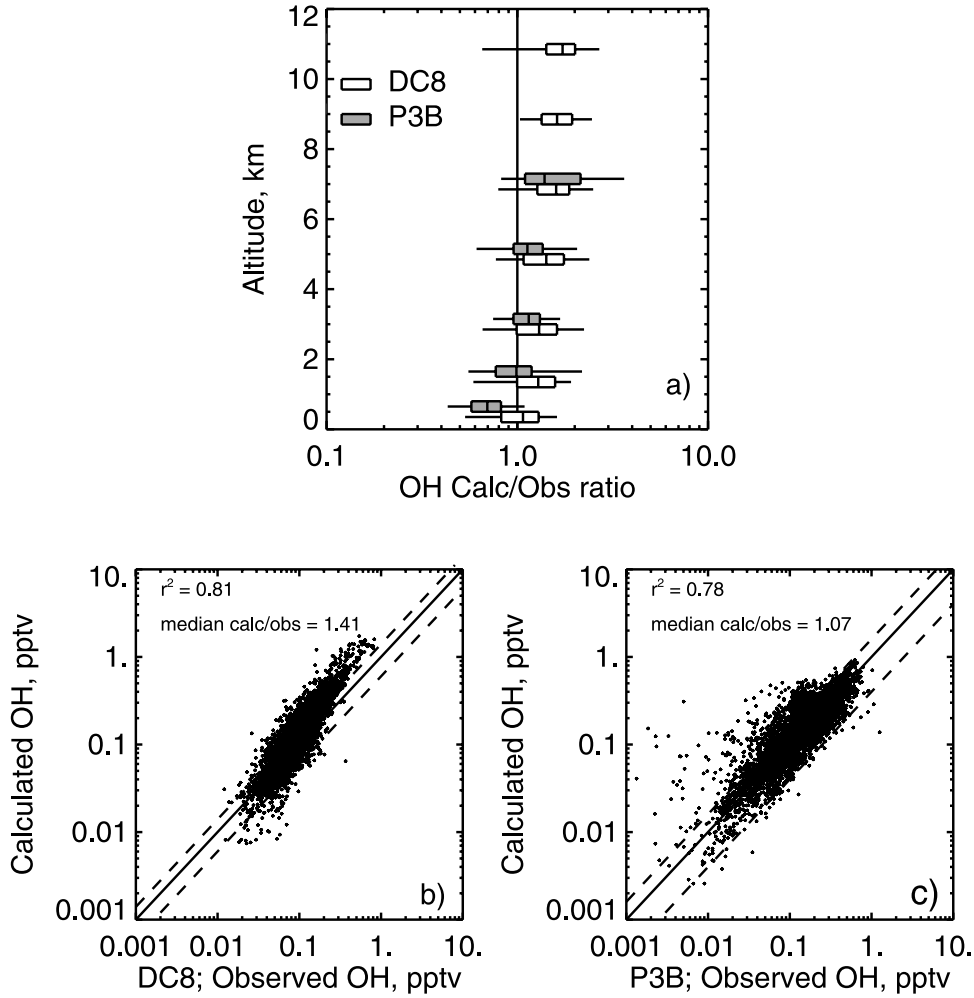

Figure 3. Comparison of calculated and observed OH from the DC-8 and P3-B aircraft. (a) Calculations of OH relative to observed values for the DC-8 (open boxes) and the P3-B (solid boxes) aircraft. See Figure 1 caption for definition of box and whiskers. Scatterplots of observed OH versus calculated OH are shown for (b) the DC-8 aircraft and (c) the P3-B aircraft. Measurement uncertainties of ±40% for the DC-8 and ±60% for the P3-B are indicated by the dashed lines in Figures 3b and 3c.

Hydrogen Oxides Sensor (ATHOS) which employs a laser induced fluorescence technique, the same instrument used during the SUCCESS, SONEX, and PEM-Tropics B field campaigns [*Brune et al.*, 1995]. Measurements of OH and HO_2 are reported at a frequency of every 10 s with an estimated absolute accuracy of 40% and a limit of detection of 0.1 pptv for HO_2 and 0.01 pptv for OH. HO_x measurements are reported for 93% of the modeled data points on the DC-8 (over 4800 points). *Eisele et al.* [2003] compare OH measurements obtained from the two aircraft from several intercomparison flights and determine that while 90% of the measurements from the two instruments agreed to within the stated instrument uncertainties, an overall bias pointed to possible problems with instrument calibration.

[21] On the DC-8, 75% of HO_2 and 48% of OH model predictions fall within the stated measurement accuracies, and 85% of the calculated P3-B OH points are within the measurement accuracy. Model-to-measurement comparisons are shown in Figure 3 for OH and in Figure 4 for HO_2. In contrast to previous campaign studies outlined above, this study shows a persistent model overprediction of DC-8 HO_2 throughout all altitudes of ~23%, with no evident altitude trend. OH is also overpredicted but with an altitude trend; the overprediction increases from 7% for altitudes below 1 km to 60% in the middle troposphere and 80% at the highest altitudes, giving an overall median overprediction of 40%. The trend in model-measurement agreement with altitude is duplicated with the P3-B OH data, though the profile is shifted toward lower ratios; boundary layer P3-B model-generated OH is underpredicted by 30% relative to measurements and is overpredicted by 40% at altitudes near 6 km [see also *Mauldin et al.*, 2003]. There was no trend in the agreement found associated with time of day (solar zenith angle).

[22] While both OH and HO_2 measured on the DC-8 have reported accuracies of ±40%, the broader range of ratios for OH reflects the lower measurement precision for this species which is derived from a much smaller signal than for HO_2 [*Faloona et al.*, 2000]. Note that the outlier points for HO_2 which fall below the agreement line at low mixing

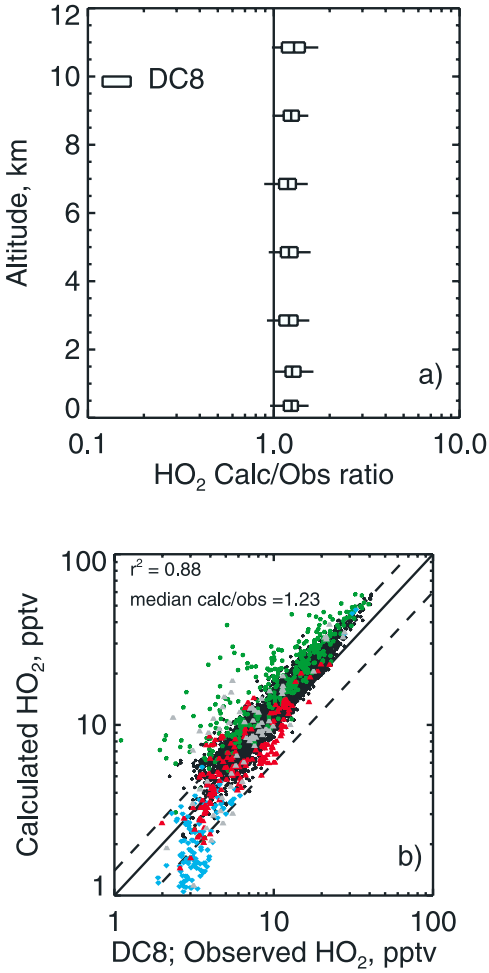

Figure 4. Comparison of calculated and observed HO_2 from the DC-8 aircraft. (a) Calculations of HO_2 relative to observed values for the DC-8 aircraft. See Figure 1 caption for definition of box and whiskers. (b) A scatterplot of observed HO_2 versus calculated HO_2 for the DC-8 aircraft. Measurement uncertainties of ±40% are indicated by the dashed lines in Figure 4b. Subsets for the HO_2 calculated-to-observed ratios discussed in the text are also indicated in Figure 4b. Blue diamonds indicate data with $O_3 > 120$ ppbv (stratospheric subset). Red triangles indicate data with NO > 135 pptv for altitudes above 7 km, and gray triangles indicate high NO data for altitudes below 7 km. Green asterisks show data points that were identified as residing in clouds, using the criteria described in the text.

ratios on Figure 4b are largely associated with stratospheric air and will be discussed section 4.1.2. Similar outlier points at low mixing ratios for the DC-8 OH (Figure 3b) are associated with higher solar zenith angles. Notably, while HO_2 on the DC-8 shows a bias of 23%, the point-to-point correspondence is quite compact ($r^2 = 0.88$).

[23] From the lack of an altitude dependence in HO_2 calculated/observed (calc/obs), it follows that the calc/obs HO_2/OH partitioning is inversely related to the altitude dependence of OH, with a 20% overprediction near the surface, decreasing to an underprediction above 8 km of 23%, a value similar to the upper tropospheric underpredictions of this ratio during SUCCESS and similar in magnitude but opposite in sign to that found during PEM-Tropics B.

4.1.2. Examination of Upper Tropospheric Outliers

[24] Three subsets of HO_2 calc/obs ratios constituting a total of 12% of the modeled HO_2 points, are identified in Figure 5a as distinct from the majority of the data. To illustrate the magnitudes of the highlighted populations, these points are also indicated in Figure 4b with the colored symbols. Subsets are defined as high O_3 or stratospheric (2.3%), high-altitude/high NO (3.3%), and in-cloud data (6.4%).

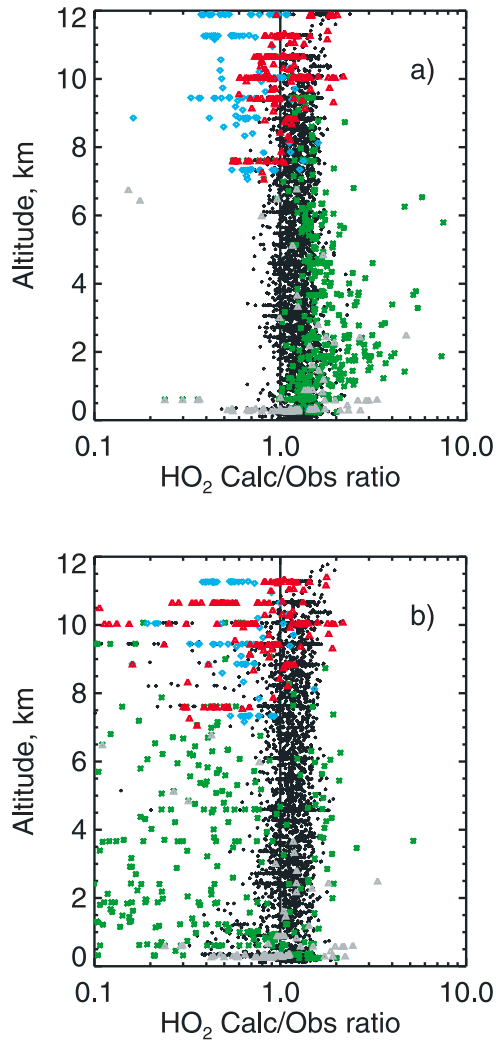

Figure 5. Subsets for HO_2 calc/obs ratios on the DC-8. (a) HO_2 calc/obs ratio versus altitude for the DC-8 aircraft. Blue diamonds indicate data with $O_3 > 120$ ppbv (stratospheric data). Red triangles indicate data with NO > 135 pptv for altitudes above 7 km, and gray triangles indicate high NO data for altitudes below 7 km. Green asterisks show data points that were identified as residing in clouds, using criteria described in the text. (b) Results from a test simulation including a heterogeneous loss of HO_2 to clouds and aerosols, so only data points containing the FSSP measurements described in the text (necessary to calculated the heterogeneous loss rate) are shown. Subsets are identified as in Figure 5a.

Table 1. Median Observations and Calculated/Observed Ratios for Subsets at Altitudes > 7 km[a]

	Majority Points	Stratospheric Points (O_3 > 120 ppbv)	High NO Points (NO > 135 pptv)
Number of points	1499	112	169
Altitude, km	9.2	10.0	10.1
Temperature, K	237	226	229
SZA, deg	42	49	36
CCF(JO^1D)	1.23	1.05	1.25
Obs HO_2, pptv	8.2	3.2	5.9
Calc/Obs HO_2	1.24	0.63	0.97
Obs OH, pptv	0.12	0.12	0.23
Calc/Obs OH	1.64	0.77	2.01
Obs HO_2/OH	70.7	25.4	25.4
Calc/Obs HO_2/OH	0.78	0.80	0.46
Obs O_3, ppbv	59	337	69
Obs CO, ppbv	102	44	118
Obs H_2O, molecules cm^{-3}	1.38×10^{15}	1.0×10^{14}	8.1×10^{14}
Obs C_2H_6, pptv	654	258	726
Obs acetone, pptv	521	164	632
Obs NO, pptv	36	75	200
Calc NO_2, pptv	12	41	40

[a]Calculated (calc) and observed (obs).

[25] Table 1 shows median observations and calc/obs ratios relevant to the two outlier subsets predominantly in the upper troposphere (>7 km): the stratospheric and high NO data points. Statistics for the remaining data points at upper altitudes are also shown, identified here as "majority data." The high O_3 points (O_3 > 120 ppbv) are shown with blue diamonds in Figures 4b and 5a, and Table 1 confirms that these points are consistent with stratospheric influence as they are associated with high O_3; low water vapor, CO, and hydrocarbons; and moderate NO_x. In contrast to the majority data, HO_x is significantly underpredicted for these stratospherically influenced points, with calc/obs values of 0.63 for HO_2 and 0.77 for OH. These points span a range of solar zenith angles (SZA) from 40° to 80°, with no correlation between the calc/obs ratio and SZA. These results are in contrast to good agreement of modeled and measured stratospheric HO_x given by *Wennberg et al.* [1998] and *Jaeglé et al.* [1997]. Note, however, that for this subset the 23% underprediction of the HO_2/OH partitioning ratio calculated for the majority subset is essentially retained, with a median underprediction of HO_2/OH of 20% (Table 1).

[26] The high NO data (NO > 135 pptv) are shown with red triangles in Figures 4b and 5a, and these points are likely associated with convected pollutants, since CO, O_3, and hydrocarbons are slightly elevated above that for the majority subset (Table 1). While the HO_2 calc/obs ratio is 0.97, it is low relative to the majority subset ratio. Note that a decrease in ratio with higher NO concentrations is consistent with the general behavior found by *Faloona et al.* [2000] on examination of SONEX and SUCCESS data. In contrast to HO_2, however, the OH calc/obs ratio for the high NO data is quite large, with a median value of 2.01. The resulting calc/obs ratio for HO_2/OH partitioning is 0.46, significantly lower than that for the stratospheric and majority subsets (0.8, see Table 1). Such behavior suggests an uncertainty related to the rate of HO_x recycling by NO. Note that data with NO > 135 pptv also occur in the lower troposphere, indicated in Figures 4b and 5a by gray triangles. However, only those high NO points at altitudes greater than ~6 or 7 km show a consistent HO_2 calc/obs behavior distinct from the preponderance of the data. Below 6 km, the median HO_2 calc/obs ratio for the high NO data is 1.23, identical to the bulk median, though there is a large scatter to the ratios. Therefore the calc/obs HO_2 discrepancy associated with high NO in this study appears limited to the upper troposphere.

[27] Selected HO_x source and loss terms are shown in Table 2 and reveal differences in the dominant instantaneous processes affecting HO_x between the subsets. For example, while the water vapor reaction with $O(^1D)$ is clearly the dominant HO_x primary source for the stratospherically influenced data, higher concentrations of acetone in the majority subset and particularly in the high NO subset results in an increased importance of acetone photolysis for those data.

[28] Because HO_x is a highly buffered system, it is difficult to significantly impact calculated HO_x by minor adjustments to the sources or losses [*Wennberg et al.*, 1998; *Crawford et al.*, 1999]. To bring the calc/obs ratio for the stratospheric HO_2 into agreement with measurements, an HO_2 increase on the order of 60% is required, and to come into agreement with the majority data subset (where the median calc/obs is 1.24) an increase on the order of 100% is required.

[29] To test the uncertainty related to water vapor measurements in stratospherically influenced air, model calculations were conducted for the stratospheric subset using water vapor measurements from a diode laser instrument, which, during dry conditions, recorded data 2.4 times larger than that from the cryogenic hygrometer, the measurement used for the base model simulations. The resulting HO_2 increase was ~17%. Similarly, because acetone photolysis is a significant primary source in the high NO subset, the uncertainty in those measurements was tested by increasing acetone by the stated measurement uncertainty of 25%. The resulting impact on HO_x is <5%.

[30] Recent studies have suggested that photodissociation of HNO_4 in the near-infrared spectrum could significantly impact the budget of HO_x, particularly in the lower stratosphere and upper troposphere [*Wennberg et al.*, 1999; *Salawitch et al.*, 2002; *Evans et al.*, 2003]. To test the potential impact of this additional photolysis, we conducted model simulations including HNO_4 near-infrared photolysis

Table 2. Selected Instantaneous HO_x Budget Terms for Subsets at Altitudes > 7 km

	Gross Production and Loss Terms, 10^3 molecules cm^{-3} s^{-1}		
	Majority Points	Stratospheric Points (O_3 > 120 ppbv)	High NO Points (NO > 135 pptv)
Model-calculated HO_x gross production			
$O^1D + H_2O$	32.3	5.3	34.0
Acetone photolysis (assume yields of 2, 3)	17.5, 26.3	1.8, 2.7	22.3, 33.4
H_2O_2 photolysis	40.7	2.5	16.0
Model-calculated HO_x gross loss			
$OH + HO_2$	41.9	3.7	53.9
$HO_2 + HO_2$	67.4	2.5	21.6
Total for HO_x-driven losses	109.3	6.2	75.5
$OH + NO_2$	2.3	4.5	17.8
Model-calculated HO_x gross production from HNO_4 cycling			
HNO_4 photolysis	2.7	3.2	6.3
HNO_4 thermal decomposition	3.4	0.9	0.9
Model-calculated HO_x gross loss from HNO_4 cycling			
$HO_2 + NO_2$	13.1	13.6	29.4
$HNO_4 + OH$	4.4	4.9	19.5

as described by *Roehl et al.* [2002]. For the stratospheric subset, median predicted HO_x increased by 17% when this photolysis was included. The impact on HO_x for the high NO subset was only ~3%, and the median impact on the majority data was negligible.

[31] Another possibility is that uncertainties in the NO measurement may have contributed to differences in the HO_2 calc/obs ratios among the subsets. Model sensitivity calculations show that an assumption of a consistent NO measurement bias of −30% is sufficient to increase predicted HO_2 within the high NO subset by 20%, resulting in a median calc/obs ratio of 1.18. Meanwhile, the impact on the majority data from this bias is limited to a few percent change in HO_2 so that differences in the calc/obs ratios between the high NO and majority subsets are no longer clearly evident. Note, however, that the distinction in the median calc/obs HO_2/OH partitioning between the two subsets remains; that is, while this assumed NO measurement bias improves the calc/obs partitioning ratio to near 1 for the majority data, a calc/obs value of 0.65 is calculated for the high NO subset. For the stratospheric subset, the impact of an assumed −30% NO measurement bias is a 27% increase in HO_2.

[32] For the stratospheric subset, the combined impact of the assumed −30% NO measurement bias, the additional HNO_4 photolysis, and the higher water vapor measurements is nonlinear, with a total increase in HO_2 of 54%, resulting in a calc/obs ratio of 0.93. Therefore, while these combined uncertainties have the potential of significantly improving the HO_2 calc/obs ratio in the stratospheric subset, the ratio remains distinct from the majority data.

[33] Additional rate sensitivity calculations were conducted to examine uncertainties in reaction rates that contribute to the loss of HO_x (see Table 2). Because HO_x self-reactions are disproportionately dominate over HNO_3 formation for the majority data relative to the stratospheric or high NO subsets, uncertainties in these rates can be expected to have a larger influence on the majority data. Holding the rates for $OH + HO_2$ and $HO_2 + HO_2$ to the higher ends of their respective uncertainties as defined by *DeMore et al.* [1997] and *Sander et al.* [2000] resulted in HO_x concentration decreases <10% larger for the majority data relative to the other subsets. Thus, though the makeup of these subsets reveals different dominating processes in the HO_x budget along with different behaviors of the HO_2 calc/obs ratios, uncertainties in primary source components or HO_x loss processes are not sufficient to explain all of the differences.

[34] Discrepancies between the stratospheric subset and the majority data subset extend beyond HO_x to CH_2O. As discussed earlier, CH_2O photolysis can be an important secondary source of HO_x in the upper troposphere; CH_2O is a photochemical byproduct of acetone and hydrocarbon degradation. For the stratospheric subset, the median measurement reported for CH_2O is 55 pptv. An important caveat to note, however, is that most of these reported values are below the instrument limits of detection (LOD) [*Fried et al.*, 2003a]. Nevertheless, this implies that measured CH_2O may be up to 3 times larger than that calculated by the model, which has a median value for the stratospheric subset of 17 pptv. If the stratospheric points are modeled while constraining CH_2O to the median measured value of 55 pptv, median predictions of OH and HO_2 increase by 71% and 79%, respectively, increasing the median OH calc/obs ratio to 1.28 and the HO_2 calc/obs ratio to 0.95. Note, however, that CH_2O levels of 55 pptv cannot be supported by the concentrations of acetone or other hydrocarbons measured.

4.1.3. Examination of In-Cloud Data

[35] The data points marked with a green asterisk in Figures 4b and 5a indicate the third subset, within-cloud data as determined by a combination of visual inspection of flight videos and measurements of particles in the 10–20 μm range from the Forward Scattering Spectrometer Probe (FSSP). Using this approach, data points were classified as in-cloud, intermediate, hazy, or clear air. There is a compelling distinction between the behaviors of calc/obs HO_2 for in-cloud points versus those in clear air, supporting a significant heterogeneous loss of HO_2 within clouds (Figure 5a). The median HO_2 calc/obs ratio for all clear air data points is 1.20, while that for in-cloud data is 25% larger, at 1.51. While the analysis of *Jaeglé et al.* [2000] suggested evidence of HO_2 heterogeneous uptake within cirrus clouds, significant model overpredictions spanned regions well outside of cloud areas as well. This data analysis shows large model overpredictions that are clearly located directly within and limited to clouds (Figure 5a). Note that the few points around 4 km that show relatively

large HO_2 calc/obs ratios and are not identified as in-cloud data are all from flight 15 and were located within the heavily polluted haze layer of the Yellow Sea; these points are all identified as either "intermediate" or "hazy" using the cloud index described above and were intermixed with points identified as "in-cloud."

[36] Further, most evidence of in-cloud HO_2 loss is limited to the lower and middle altitudes. For data points within clouds at altitudes below 6 km, the HO_2 calc/obs ratio is 1.55, while that for in-cloud points above 6 km is 1.32. Contrary to previous studies [e.g., *Jaeglé et al.*, 2000], this suggests that cloud uptake plays only a minor role in upper tropospheric HO_x chemistry.

[37] To expand the investigation of heterogeneous impacts to aerosol in both cloudy and in clear air, a theoretical heterogeneous loss of HO_2 was added to the model. The heterogeneous loss rate (k_{het}) is parameterized as

$$k_{het} = \int_{a_{min}}^{a_{max}} \frac{n(a)4\pi a^2}{\left(\frac{a}{D_g} + \frac{4}{\upsilon\gamma}\right)} da, \quad (2)$$

where a is the effective particle radius for a given observational size bin, $n(a)$ is particle number size distribution, D_g is the gas-phase molecular diffusion coefficient of HO_2, υ is the mean molecular speed, and γ is a reaction probability which is set to 0.2, as suggested by *Jacob* [2000]. The integral is evaluated over all the available particle size spectrum observations by the FSSP and optical particle counter instruments on board the DC-8 aircraft. The observations are reported in six size bins and span the size range of 0.1–50 μm. The median decrease in calculated HO_2 due to in-cloud heterogeneous loss is 70%, reducing the median in-cloud calc/obs HO_2 ratio to 0.42 (Figure 5b, green asterisks). Thus the loss calculated using the simple parameterization in equation (2) is shown to be quantitatively inconsistent with that suggested by these observations. However, note that the error in estimated cloud aerosol number/size distribution data is on the order of 100% so the parameterization is highly uncertain, and there may be additional HO_2 loss limiting factors which are not described in equation (2). Furthermore, heterogeneous losses to HO_x precursors and/or reservoir species were not considered in this assessment (e.g., CH_2O and H_2O_2 [see *Fried et al.*, 2003a]).

[38] The estimated impact on HO_2 from heterogeneous loss to aerosol in clear air (no cloud) can also be seen in Figure 5b and is calculated to be on the order of a 4% decrease, with minimum decreases in the upper troposphere (1–2%) and maximum decreases in the boundary layer (12%). The boundary layer heterogeneous losses therefore could explain about half of the median model boundary layer overestimate; however, the HO_2 measurement is not sensitive enough to independently verify the existence or magnitude of this HO_2 loss.

4.2. Formaldehyde

[39] Measurement-to-model comparisons of CH_2O have a long history, particularly in the remote troposphere. Such comparisons have exhibited both positive and negative deviations, as well as good agreement. In the marine boundary layer, models have overpredicted CH_2O relative to measurements [*Lowe and Schmidt*, 1983; *Jacob et al.*, 1996; *Liu et al.*, 1992; *Zhou et al.*, 1996] as well as underpredicted CH_2O [*Weller et al.*, 2000; *Ayers et al.*, 1997]. Models have typically underpredicted CH_2O in the middle and upper troposphere [*Jaeglé et al.*, 2000; *Heikes et al.*, 2001; *Fried et al.*, 2002; *Frost et al.*, 2002]. Two recent studies have shown good agreement on average between CH_2O model predictions and measurements: *Fried et al.* [2003b] during the Tropospheric Ozone Production about the Spring Equinox (TOPSE) 2000 airborne campaign, and the shipboard studies by *Wagner et al.* [2002]. *Wagner et al.* [2002] also presented results from a conservative uncertainty analysis of both theory and measurements which concluded that deviations between models and measurements as large as 65% were not significant for the MBL data they interpreted.

[40] During TRACE-P, two independent instruments measured formaldehyde on board the DC-8: a coil enzyme method [*Heikes et al.*, 1996] and a tunable diode laser absorption spectrometer [*Fried et al.*, 2003a]. Measurements from the coil enzyme method [*Heikes et al.*, 1996] are on the order of ~30% higher than the laser spectrometer [*Fried et al.*, 2003a]. A more detailed comparison of the two CH_2O measurements is presented by *Eisele et al.* [2003]; 60% of the compared points fall within measurement uncertainties. For this analysis, we focus on model comparisons with data from the laser spectrometer, which has a data coverage much larger than that from the coil enzyme. Note that a CH_2O model-measurement comparison using these data and model results are also discussed by *Fried et al.* [2003a].

[41] Values of the 2σ LOD for the laser spectrometer were typically between 60 and 80 pptv [*Fried et al.*, 2003a], and one third of all measured CH_2O was at LOD. This percentage is greatest at upper altitudes, with 60% of the measurements above 8 km below LOD. As discussed by *Fried et al.* [2003a], CH_2O concentrations are reported for all data, including those at and below LOD. Though these LOD data are, by definition, are too noisy to give information on a point-by-point basis, by including their statistical impact in the running median, we are able to avoid biasing our comparison at the low end of the concentration range.

[42] A scatterplot of modeled versus observed formaldehyde is shown in Figure 6a, with a smoothed version of the data used in Figure 6b. Note that some of the data below LOD were reported as negative and do not appear on these logarithmic plots. To create the smoothed data, measurement-model data pairs were first sorted by model concentration, and measurements were then smoothed using a 1% running average. By sorting the data pairs using model concentration rather than measurement, the smoothing process eliminates negative values and allows for an assessment of the reported LOD.

[43] For the full raw data set (Figure 6a), the median calc/obs ratio for CH_2O is 0.92, with an r^2 correlation coefficient of 0.85. However, the general behavior of the calculated-to-observed comparison differs distinctly across the spectrum of measured CH_2O mixing ratios. This behavior within the data is more clearly evident when smoothing the data (Figure 6b). In Figure 6b, calculated CH_2O agrees well with observed values for mixing ratios of roughly 60–500 pptv. Here, the slope of the agreement equals 1.02,

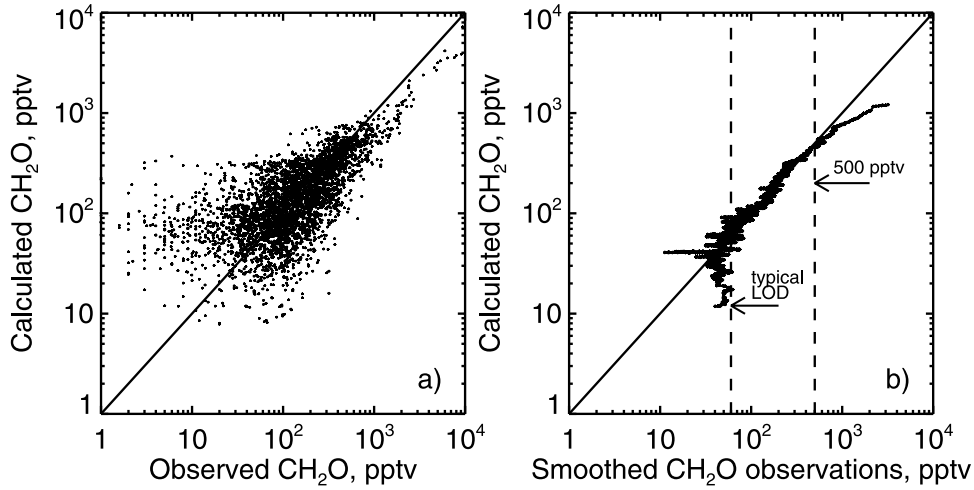

Figure 6. Comparison of calculated and observed CH_2O from the DC-8. (a) Scatterplot of observed versus calculated CH_2O from the DC-8. The agreement line is shown with a solid line. Note that data reported as negative do not appear on the logarithmic scale. (b) Smoothed version of the observed CH_2O versus calculated values. The smoothed data were created by sorting the measurement-model pairs based on model concentration, and measurements were then smoothed using a 1% running average. The reported typical LOD value of 60 pptv is indicated with a dashed line, and the 500 pptv concentration level is also indicated with a dashed line. The agreement line is shown with the solid line.

indicating no bias in the model-to-measurement comparison. These results corroborate those shown by *Fried et al.* [2003a], who employ a binned regression analysis approach. Below ~60 pptv, the measurement-model correlation degrades for this comparison, which agrees with the reported 1-min LOD of *Fried et al.* [2003a]. Note, however, that as discussed by *Fried et al.* [2003a], longer measurement averages can, in some instances, be employed during stable horizontal flight legs to improve the measurement precision. For concentrations >500 pptv, the slope differs markedly, with a value of 0.37, as the model increasingly underpredicts CH_2O at the highest concentrations.

4.2.1. Impact of Transport on CH_2O Predictions

[44] One explanation for the underprediction of CH_2O at highest concentrations is that direct transport of CH_2O and its precursors (such as ethene or methanol) can shift the concentration of CH_2O away from photochemical steady state. However, because the median lifetime of CH_2O for the daylight TRACE-P calculations is 2.2 hours, evidence of transport influence on these calculations of CH_2O is expected to be limited to within a few hours of large emission areas. Note that the transport impact distance would increase for nighttime emissions, when the instantaneous CH_2O and precursor lifetime is longer.

[45] Figure 7 shows the geographical locations of high-concentration CH_2O measurements and of significant model underestimations. Figure 7a shows the location of all CH_2O measurements, and in Figure 7b, all measurements >500 pptv, constituting ~7% of the data, are identified. While several isolated measurements exceed 500 pptv, given the scatter seen in Figure 6a, it is difficult to arbitrate the model versus measurement disagreement. Therefore extended periods of high CH_2O concentration (>500 pptv) are identified based on averaging over horizontal flight legs (Figure 7c). These occurrences reduce the number of identified points to 3% of the data set and are limited to the Yellow Sea and a few locations farther offshore. Figure 7d shows points within these identified flight legs for which the calc/obs ratio is <0.7, which constitute ~1% of the total CH_2O observations. For the remainder of points with flight leg averages larger than 500 pptv, the median calc/obs ratio is 0.96, indicating no substantial bias in the model prediction. The fact that the large underpredictions are exclusively located in the Yellow Sea and at altitudes below 2.5 km suggests the possibility of transport influence. However, back trajectories using Hybrid Single-Particle Lagrangian Integrated Trajectory (HYSPLIT, http://www.arl.noaa.gov/ready/hysplit4.html, NOAA Air Resources Laboratory, Silver Spring, Maryland) run from the locations in Figure 7d show that while slightly more than half of these observations were subjected to <6 hours of day lit transport time from the coast, the remainder indicated transport times in excess of 1 day. This qualitative examination suggests that during the overall TRACE-P campaign, transport influences on CH_2O, while probably present, were quite rare, impacting on the order of only a few percent of the data at most.

[46] To further verify the diurnal steady state assumption for CH_2O, an exercise was undertaken using results from version 4.33 of the Harvard 2 × 2.5 GEOS-CHEM global model simulation for the TRACE-P time period in place of observational data (http://www-as.harvard.edu/chemistry/trop/geos/geos_version.html; M. Evans et al., manuscript in preparation, 2004). The box model analysis was repeated using GEOS-CHEM global model parameters from along simulated flight tracks through the model environment as box model constraints, and box model predictions for formaldehyde, based on diurnal photochemical steady state, were then compared to those predicted by GEOS-CHEM, which includes simulated effects of both photochemistry and transport. The resulting median box model/GEOS-CHEM CH_2O ratio is 0.92, a bias determined to be a result

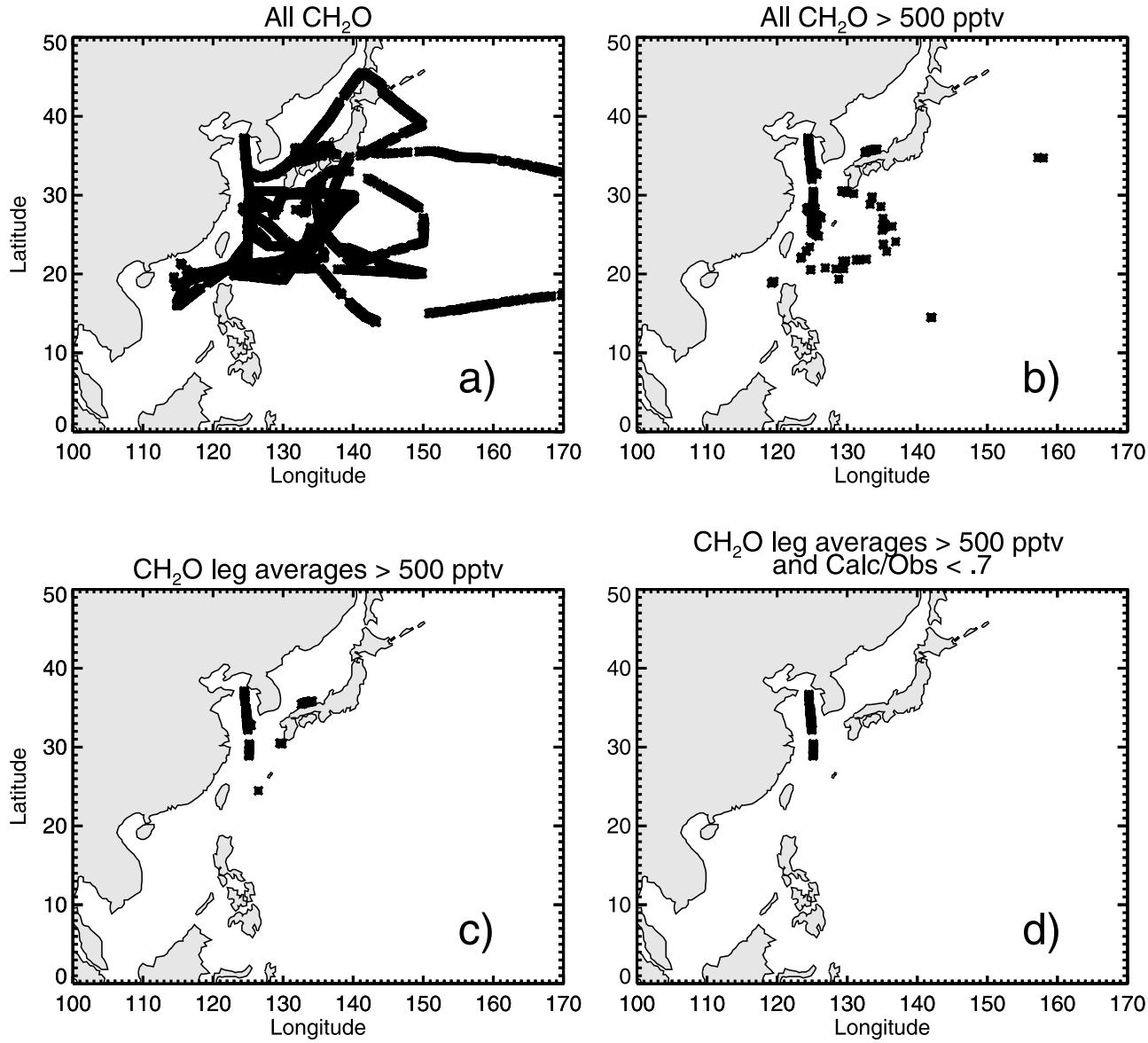

Figure 7. Geographical locations of CH_2O measurements during TRACE-P. (a) Latitude/longitude location of all CH_2O measurements by the laser spectrometer during TRACE-P. (b) Measurements >500 pptv. (c) Points where CH_2O averages over horizontal flight legs are >500 pptv. (d) Points where flight legs averages are >500 pptv and where the calc/obs ratio is <0.7.

of minor input and mechanistic differences between the two models. The agreement between the two models is compact, however (r^2 = 0.93), which supports the assumption of steady state for formaldehyde throughout most of the TRACE-P region. Figure 8a shows the box model/GEOS-CHEM CH_2O ratios for the upper 50th percentile of the GEOS-CHEM concentrations, while a similar plot for the calc/obs ratio using observational data is shown in Figure 8b. Median ratios for segments of tenths of percentiles are indicated near the top of Figures 8a and 8b. The uppermost 10th percentile segment ratio for GEOS-CHEM decreases abruptly from 0.91 to 0.85, similar to but not as pronounced as the decrease to 0.69 for the upper 10th percentile of observed data.

[47] Similar to results described for the observations, large box model underpredictions (calc/obs < 0.7) of high concentrations of GEOS-CHEM CH_2O (>500 pptv) constitute only 1.1% of the Harvard data set. About half of these identified points reside near coastal regions in the Yellow Sea or off the coast of Taiwan, with the remainder located more than a day's transport time from the coast. Therefore, while the box model analyses using both the observational data and the GEOS-CHEM analysis suggest that there are isolated cases where transport may influence CH_2O, these cases are rare, with the portion of the data affected on the order of a few percent or less.

4.2.2. Impact of Constraining Species on the Model-Measurement Comparison

[48] Agreement between calculations and observations is quite good for CH_2O data falling between the measurement LOD and 500 pptv, but this agreement is not readily apparent without smoothing the data. The comparison in

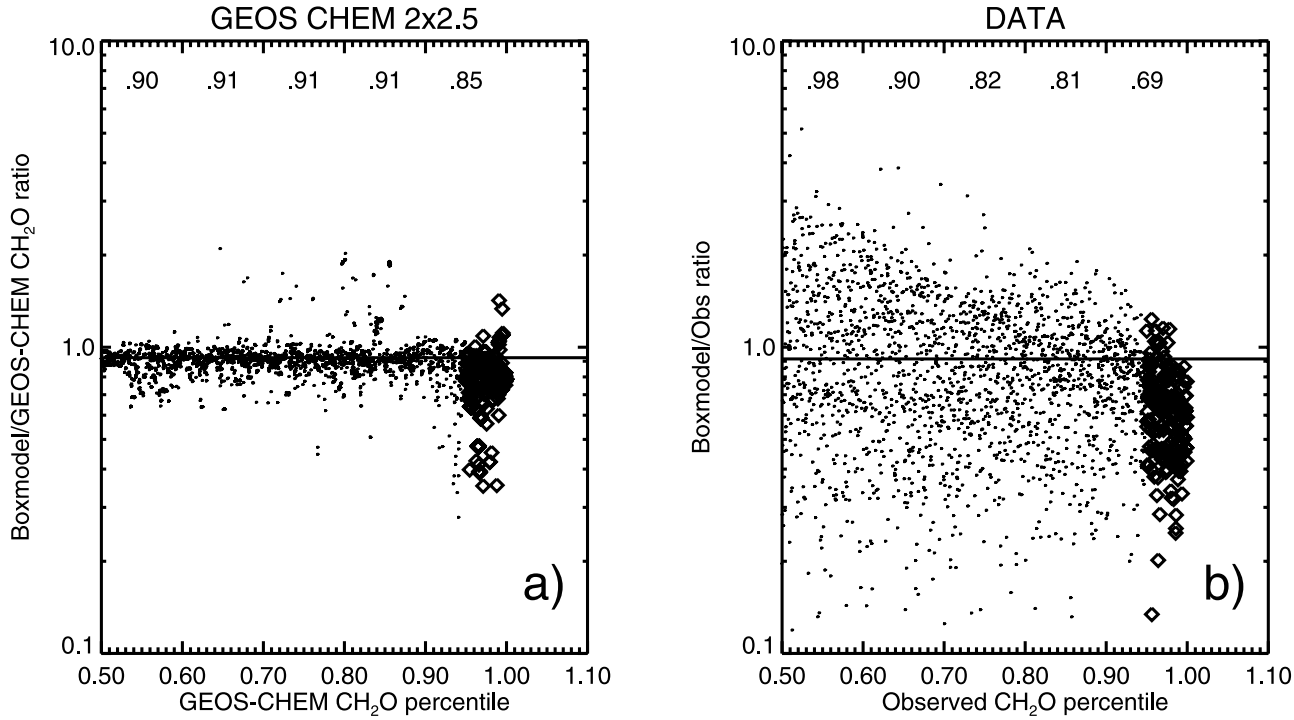

Figure 8. Comparison of box model predictions of CH_2O versus GEOS-CHEM and versus observational data from TRACE-P. (a) Plot with the x axis showing the upper 50th percentile of concentrations of CH_2O in the GEOS-CHEM along simulated TRACE-P flight tracks and the y axis showing the CH_2O box model/GEOS-CHEM ratio for those points. The solid line shows the median box model/GEOS-CHEM ratio for the entire data set. Numbers along the top portion indicate median ratios for the 10th percentile segments along the concentration range. Open diamonds indicate the upper 5th percentile of the GEOS-CHEM data. (b) Same as Figure 8a except for observed CH_2O during TRACE-P and the corresponding box model predictions.

Figure 6a is quite scattered for data below 500 pptv (r^2 = 0.46), and this noise is likely to be due to a variety of causes. Some of these include uncertainties in the measurement (2σ LOD $\sim$ 60–80 pptv) or in the model mechanism, uncertainties in the modeling approach (e.g., treatment of clouds), and uncertainties in formaldehyde precursors, which encompass both the limited availability of precursor constraints and also measurement issues (e.g., unmeasured hydrocarbon species or uncertainties in measurements of precursors such as CH_3OOH). *Fried et al.* [2003a] also discuss some aspects of measurement and model uncertainties.

[49] As noted earlier, this modeling study is limited by the availability of several important but noncritical model inputs (H_2O_2, CH_3OOH, PAN, and HNO_3), which are constrained to observations at points where data are available and are calculated where observations are missing. The uncertainty imposed by the limited availability of these constraining species becomes most obvious in calculations for periods of flight through homogeneous air masses. If model predictions of these species are significantly different than adjacent measurements, the resulting fluctuations in the flight data time series between the measured value (when available) and the calculated value can be large. Depending on the sensitivity of CH_2O to variations in these constraining species, this in turn can potentially introduce noise into the time series of calculated CH_2O; this is particularly so for CH_3OOH. Further complicating things, some of these periods of large fluctuations between adjacent measurements and calculations for CH_3OOH in the TRACE-P data are seen where the presence of a constraining measurement improves model-measurement agreement for CH_2O while other periods clearly exhibit better agreement when constraining species are absent. This type of behavior is also described by *Fried et al.* [2003a].

[50] To evaluate the sensitivity of CH_2O to the availability of noncritical constraint species, we conducted several independent model tests. For each noncritical constraint species, a set of model simulations was conducted with the test species calculated, rather than constraining it to the observed value. Differences in predictions of CH_2O were then examined as a function of the differences in the calculated and observed values of the test species. The total dynamic range of model over and under predictions was similar for all of the constraint species. The impacts of HNO_3, H_2O_2, and PAN constraints on CH_2O were relatively low. The sensitivity of CH_2O to HNO_3 was always <2% and was <20% for H_2O_2 and PAN.

[51] In contrast, the response in CH_2O to variations in CH_3OOH were large. Results from test simulations for CH_3OOH are shown in Figure 9. The x axis on Figure 9a shows CH_3OOH calc/obs ratios, with values greater than one indicating a model overprediction, and the y axis shows

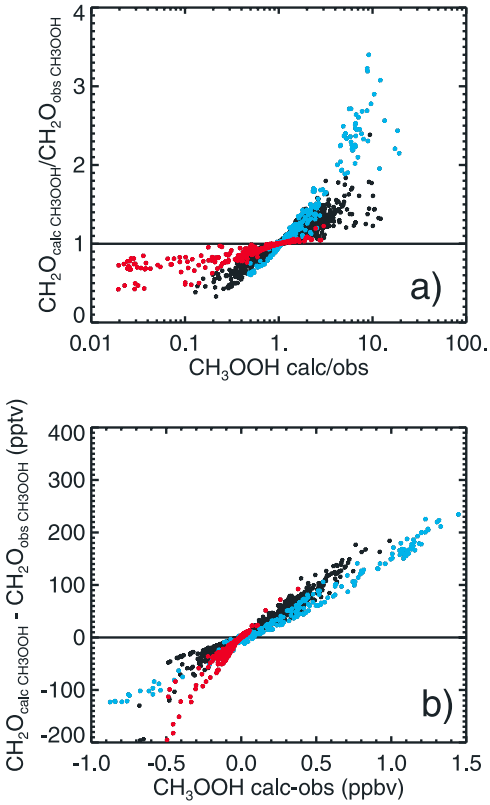

Figure 9. Impact of CH_3OOH constraints on CH_2O. (a) The calc/obs ratios of CH_3OOH on the x axis and the resulting relative change in predictions of CH_2O on the y axis. Values of calc/obs CH_3OOH > 1 indicate a model overprediction. (b) Absolute differences (calculated minus observed) with the associated absolute difference in predicted CH_2O. Red symbols indicate where NO was >50 pptv, and blue symbols indicate where NO was <5 pptv.

the resulting relative differences in predicted CH_2O. While the median CH_3OOH calc/obs ratio is 1.06, the agreement is altitude-dependent. Below 4 km, there is a median overprediction of 40–50%, and above 8 km, there is a median underprediction of 40. Figure 9b shows absolute differences for CH_3OOH (calc-obs) and for resulting predictions of CH_2O. The response in CH_2O, with absolute differences of several hundred parts per trillion by volume and relative ratios ranging from 0.3 to 3.5, may be interpreted as a measure of the variance potentially introduced as a result of the limited availability of CH_3OOH.

[52] The colors in Figure 9 indicate the level of NO; blue points show data where NO was <5 pptv, and red points show data where NO was measured at >50 pptv. Figure 9a indicates that CH_2O is particularly sensitive to CH_3OOH when NO levels are very low. Under these conditions, formaldehyde production becomes dominated by photolysis of CH_3OOH as the production from the methyl peroxy radical reaction with NO becomes small. Note that CH_3OOH is frequently overpredicted by the model under low NO conditions (i.e., 80% of the blue points in Figure 9a are greater than one). One possible explanation for this is a box model overestimation of the peroxy radical production of CH_3OOH by the steady state approach which neglects any time evolution of intermediate-lived species such as NO_x, particularly in the presence of upstream emissions. A similar effect is also suggested by *Wang et al.* [2002] in a steady state box model analysis using data over the northern and middle high latitudes from the TOPSE field campaign. Additionally, *Fried et al.* [2003a] propose the possibility that reactions of CH_3OOH on aerosols and/or with halogens may be important and result in model underpredictions of this species under low NO conditions.

[53] While these exercises illustrate the theoretical sensitivity of CH_2O predictions to CH_3OOH, it is useful to determine how often the large fluctuations actually occur in the field data and whether the resulting introduction of noise impacts the gross statistics of the CH_2O comparison seen in Figure 6. Within the lowest 2 km, we identified 175 CH_2O data points that were located within seven constant-altitude legs where differences in calculated and observed CH_3OOH were at least 250 pptv and where resulting model predictions of CH_2O differed by at least 30%. These 175 flagged points constitute ~13% of all CH_2O data at those altitudes. Above 2 km, such fluctuations are much rarer; affecting only ~2% of the data. The overall median CH_2O calc/obs ratio for altitudes below 2 km is 1.03, with a calculated versus observed r^2 correlation of 0.2. For the subset of these points with observations of CH_3OOH, the median calc/obs CH_2O decreases to 0.91, and for the subset of points using calculated CH_3OOH, the median ratio increases to 1.12. While this establishes that limited observations of CH_3OOH is a source of uncertainty in model calculations versus observations, it is interesting to further note that the r^2 correlation between model predictions and observations of CH_2O remains unchanged when limiting the comparison to either of the subsets using observations or calculations of CH_3OOH. Thus other sources of uncertainty must dominate the scatter for the CH_2O comparison seen in Figure 6. These of course include uncertainty in both the CH_2O measurements themselves as well as the uncertainty in constraining measurements. What is clear from this exercise is the sensitivity of CH_2O predictions to presumed concentrations of CH_3OOH. Therefore, in order to more accurately assess formaldehyde measurements, accurate measurements of CH_3OOH, particularly in low NO_x regimes, are critical.

4.2.3. Impact of Clouds on Predictions of CH_2O

[54] *Fried et al.* [2003a] discuss the role of local in-cloud heterogeneous loss of CH_2O. This in situ loss is not specifically reproduced by the box model, which assumes a climatological wet loss throughout the troposphere but does not simulate instantaneous in-cloud removal. *Fried et al.* [2003a] conclude that model predictions of CH_2O can be up to 56% larger than observed within cloudy regions as a result of this effect.

[55] Another impact related to clouds that affects predictions of CH_2O is the application of the cloud correction factor (CCF; see section 2). For example, at very low or very high CCF (i.e., when in an environment with heavy cloud attenuation or high reflectance), the assumption that these extreme cloud influences persist throughout the diurnal cycle is most likely erroneous. Approximately 10% of CH_2O data below 500 pptv fall under these extreme conditions, identified as CCF (JO^1D) <0.5 or >1.7. For CCF (JO^1D) values <0.5, CH_2O is underpredicted, with a median calc/obs ratio of 0.67, and for CCF (JO^1D) >1.7, the median

calc/obs ratio is 1.3, indicating a model overprediction. However, when removing extreme CCF data and in-cloud data points (identified as described in section 4.1.3) from the analysis, the correlation coefficient between calculated and observed CH_2O is essentially the same (0.46 versus 0.49), and the median calc/obs ratio is unchanged from the bulk value. This suggests that the assumption of diurnal persistence of clouds, while clearly introducing uncertainty, does not introduce bias into the comparison, and is insufficient to explain the large amount of scatter in agreement seen in Figure 6a.

5. Summary

[56] Model predictions of HO_x showed good agreement relative to measurements from TRACE-P; 75% of OH and HO_2 predictions for DC-8 data fell within the stated instrument uncertainties, and 85% of the P3-B OH predictions were within the stated uncertainties. HO_x was generally overpredicted throughout the troposphere, in contrast to results from several previous field campaigns. The calc/obs ratio for OH on the DC-8 indicated a median overprediction of 40% and a trend with altitude; measurements were overpredicted by 7% at altitudes below 1 km, increasing to a 80% overprediction at the highest altitudes. This trend was duplicated with the P3-B OH data, though shifted toward lower ratios, with boundary layer OH underpredicted by 30% relative to measurements and overpredictions of 40% at 6 km altitude. The calc/obs ratio for HO_2 on the DC-8 showed a consistent 23% model overprediction bias throughout all altitudes and a high point-to-point correspondence, with a correlation coefficient (r^2) of 0.88. Three subsets stood out as distinct from the preponderance of the data, however: stratospherically influenced data, upper tropospheric data with high NO (>135 pptv), and data obtained within clouds.

[57] Median HO_2 calc/obs ratios in the stratospheric subset were quite low (0.63) relative to a median ratio of 1.24 for the majority data. Likewise, the stratospheric median OH calc/obs ratio was also low, with a value of 0.77 relative to 1.81 for the majority data. These findings are in contrast to previous studies of stratospheric OH which indicated good agreement between models and measurements [e.g., *Wennberg et al.*, 1998; *Jaeglé et al.*, 1997]. Several sensitivity studies were conducted to examine influences on HO_x pertinent to the stratospheric subset. Even with the combined effects of an increase in stratospheric water vapor by a factor of 2.4 to measurements taken from the laser hygrometer, the inclusion of the near-IR HNO_4 photolysis [*Roehl et al.*, 2002], and an assumed −30% NO measurement bias, the resulting increase in predicted HO_2 within the stratospheric subset of 54% was not sufficient to explain the disconnect from the majority data.

[58] The subset with high NO (>135 pptv) in the upper troposphere had a median HO_2 calc/obs ratio of 0.97, also lower than the 1.24 ratio for the majority data. A tendency for a lower HO_2 calc/obs ratio with higher NO is consistent with findings by *Faloona et al.* [2000] during the SUCCESS and SONEX field campaigns. In contrast, OH was overpredicted in this subset by a median calc/obs ratio of 2.01, compared to the majority data OH calc/obs ratio of 1.81. The resulting HO_x partitioning ratio (HO_2/OH) was therefore underpredicted, with a calc/obs value of 0.46. This is significantly lower than that for the stratospheric and majority data (both equal to 0.8), suggesting an uncertainty related to the rate of HO_x recycling by NO. While the assumed −30% bias in the NO measurement resulted in a 20% increase in predicted HO_2 for this subset, the impact on the majority data was minimal, so that the distinction between calc/obs HO_2 for these two subsets was no longer evident. However, differences in the calc/obs HO_x partitioning remained, with an increase in the ratio to near 1 for the majority data versus a value of 0.65 for the high NO subset.

[59] The third subset included data obtained within clouds. Elevated calc/obs HO_2 ratios were directly correlated to in-cloud data at lower and middle altitudes. The median in-cloud HO_2 ratio below 6 km was 1.55, substantially higher than that for data identified as in clear air (1.20). There was no evidence of significant HO_2 uptake within cirrus and other high-altitude clouds (above 6 km), however, which is a result in contrast to previous studies suggesting a significant loss of HO_2 to cirrus clouds [e.g., *Jaeglé et al.*, 2000]. Heterogeneous loss of HO_2 to aerosol outside of clouds had a much smaller impact on HO_2, and these HO_2 measurements are not sensitive enough to independently verify the magnitude of this HO_2 loss.

[60] Measurements of formaldehyde from the tunable diode laser absorption spectrometer were compared to model predictions. Similar to previous analyses, methanol observations were shown to increase predicted CH_2O by ∼10% throughout the TRACE-P domain. The median calc/obs agreement was very good for data falling between the measurement LOD and 500 pptv, with a value of 1.02. However, the agreement was marked by large scatter (r^2 = 0.46). The general behavior of the model-to-measurement comparison differed across the spectrum of measured CH_2O mixing ratios, however. For concentrations >500 pptv (∼7% of the data), the model increasingly underpredicted CH_2O with a median ratio of 0.66. While some transport influences on CH_2O are evident in the data, it was found that no more than a few percent of the data set could be conclusively determined to be impacted by transport. These conclusions were further supported by a test of the steady state assumption for CH_2O using a simulation of TRACE-P conditions by the Harvard GEOS-CHEM global model in place of the real atmosphere.

[61] For the CH_2O data between LOD and 500 pptv, the large scatter is likely due to a variety of causes, including finite measurement imprecision (2σ LOD ∼ 60–80 pptv), uncertainties in the modeling approach (e.g., treatment of clouds), and uncertainties in CH_2O precursors, encompassing issues such as the limited availability of precursor measurements and also measurement issues such as unmeasured hydrocarbon species or uncertainties in measurements of precursors such as CH_3OOH. Specifically, CH_2O was determined to be quite sensitive to CH_3OOH, particularly at low altitudes and under low NO_x conditions where predicted CH_2O could vary by more than a factor of 2 (several hundred parts per trillion by volume) as a result of the differences between measured and predicted CH_3OOH. During TRACE-P, ∼13% of the CH_2O data was impacted by the limited availability of CH_3OOH measurements. However, correlation between model predictions and measurements did not improve when limiting the analysis

to only those points with measured CH_3OOH, suggesting that other uncertainties must play a dominant role. Similarly, while clouds were shown to introduce some uncertainty due to potential heterogeneous losses of CH_2O and also due to the assumption of diurnal persistence of extreme local radiative deviations, these effects did not introduce bias into the model-to-measurement comparison. Further, the removal of those points had no impact on the calculated correlation between model predictions and measurements.

[62] **Acknowledgments.** This work was supported by the NASA Tropospheric Chemistry Program. The authors would also like to thank the pilots and crew of the NASA's DC-8 and P3-B aircraft for their efforts in support of the TRACE-P flights.

References

Atkinson, R., D. L. Baulch, R. A. Cox, R. F. Hampson Jr., J. A. Kerr, and J. Troe (1992), Evaluated kinetic and photochemical data for atmospheric chemistry, Supplement IV, IUPAC subcommittee on gas kinetic data evaluation for atmospheric chemistry, *J. Phys. Chem. Ref. Data*, *21*, 1125–1568.

Ayers, G. P., R. W. Gillett, H. Granek, C. de Serves, and R. A. Cox (1997), Formaldehyde production in clean marine air, *Geophys. Res. Lett.*, *24*, 401–404.

Brune, W. H., P. S. Stevens, and J. H. Mather (1995), Measuring OH and HO_2 in the troposphere by laser-induced fluorescence at low pressure, *J. Atmos. Sci.*, *52*, 3328–3336.

Brune, W. H., et al. (1998), Airborne in-situ OH and HO_2 observations in the cloud-free troposphere and lower stratosphere during SUCCESS, *Geophys. Res. Lett.*, *25*, 1701–1704.

Brune, W. H., et al. (1999), OH and HO_2 chemistry in the North Atlantic free troposphere, *Geophys. Res. Lett.*, *26*, 3077–3080.

Cantrell, C., et al. (2003), Peroxy radical behavior during TRACE-P as measured aboard the NASA P-3B aircraft, *J. Geophys. Res.*, *108*(D20), 8797, doi:10.1029/2003JD003674.

Chen, G., et al. (2001), An assessment of HO_x chemistry in the tropical Pacific boundary layer: Comparison of observations with model simulations during PEM Tropics A, *J. Atmos. Chem.*, *38*, 317–344.

Crawford, J., et al. (1999), Assessment of upper tropospheric HO_x sources over the tropical Pacific based on NASA GTE/PEM data: Net effect on HO_x and other photochemical parameters, *J. Geophys. Res.*, *104*, 16,255–16,273.

Davis, D. D., et al. (2003), An assessment of western North Pacific ozone photochemistry based on springtime observations from PEM-West B (1994) and TRACE-P (2001) field studies, *J. Geophys. Res.*, *108*(D21), 8829, doi:10.1029/2002JD003232.

DeMore, W. B., S. P. Sander, D. M. Golden, R. F. Hampson, M. J. Kurylo, C. J. Howard, A. R. Ravishankara, C. E. Kolb, and M. J. Molina (1997), Chemical kinetics and photochemical data for use in stratospheric modeling, *JPL Publ.*, *97-4*.

Eisele, F. L., et al. (2003), Summary of measurement intercomparisons during TRACE-P, *J. Geophys. Res.*, *108*(D20), 8791, doi:10.1029/2002JD003167.

Evans, J. T., M. P. Chipperfield, H. Oelhaf, M. Stowasser, and G. Wetzel (2003), Effect of near-IR photolysis of HO_2NO_2 on stratospheric chemistry, *Geophys. Res. Lett.*, *30*(5), 1223, doi:10.1029/2002GL016470.

Faloona, I., et al. (2000), Observations of HO_x and its relationship with NO_x in the upper troposphere during SONEX, *J. Geophys. Res.*, *105*, 3771–3784.

Fried, A., Y.-N. Lee, G. Frost, B. Wert, B. Henry, J. R. Drummond, G. Hubler, and T. Jobson (2002), Airborne CH_2O measurements over the North Atlantic during the 1997 NARE campaign: Instrument comparisons and distributions, *J. Geophys. Res.*, *107*(D4), 4039, doi:10.1029/2000JD000260.

Fried, A., et al. (2003a), Airborne tunable diode laser measurements of formaldehyde during TRACE-P: Distributions and box-model comparisons, *J. Geophys Res.*, *108*(D20), 8798, doi:10.1029/2003JD003451.

Fried, A., et al. (2003b), Tunable diode laser measurements of formaldehyde during the TOPSE 2000 study: Distributions, trends, and model comparisons, *J. Geophys. Res.*, *108*(D4), 8365, doi:10.1029/2002JD002208.

Frost, G. J., et al. (2002), Comparisons of box model calculations and measurements of formaldehyde from the 1997 North Atlantic Regional Experiment, *J. Geophys. Res.*, *107*(D8), 4060, doi:10.1029/2001JD000896.

Heikes, B. G., et al. (1996), Hydrogen peroxide and methylhydroperoxide distributions related to ozone and odd hydrogen over the North Pacific in the fall of 1991, *J. Geophys. Res.*, *101*, 1891–1905.

Heikes, B., J. Snow, P. Egli, D. O'Sullivan, J. Crawford, J. Olson, G. Chen, D. Davis, N. Blake, and D. Blake (2001), Formaldehyde over the central Pacific during PEM-Tropics B, *J. Geophys. Res.*, *106*, 32,717–32,731.

Jacob, D. J. (2000), Heterogeneous chemistry and tropospheric ozone, *Atmos. Envivron.*, *34*, 2131–2159.

Jacob, D. J., et al. (1996), Origin of ozone and NO_x in the tropical troposphere: A photochemical analysis of aircraft observations over the south Atlantic basin, *J. Geophys. Res.*, *101*, 24,235–24,250.

Jaeglé, L., et al. (1997), Observed OH and HO_2 in the upper troposphere suggest a major source from convective injection of peroxides, *Geophys. Res. Lett.*, *24*, 3181–3184.

Jaeglé, L., D. J. Jacob, W. H. Brune, D. Tan, I. Faloona, A. J. Weinheimer, B. A. Ridley, T. L. Campos, and G. W. Sachse (1998), Sources of HO_x and production of ozone in the upper troposphere over the United States, *Geophys. Res. Lett.*, *25*, 1705–1708.

Jaeglé, L., et al. (2000), Photochemistry of HO_x in the upper troposphere at northern midlatitudes, *J. Geophys. Res.*, *105*, 3877–3892.

Lee, M., B. G. Heikes, D. J. Jacob, G. Sachse, and B. Anderson (1997), Hydrogen peroxide, organic hydroperoxide, and formaldehyde as primary pollutants from biomass burning, *J. Geophys. Res.*, *102*, 1301–1309.

Liu, S. C., et al. (1992), A study of the photochemistry and ozone budget during the Mauna Loa Observatory Experiment, *J. Geophys. Res.*, *97*, 10,463–10,471.

Logan, J. A., M. J. Prather, S. C. Wofsy, and M. B. McElroy (1981), Tropospheric chemistry: A global perspective, *J. Geophys. Res.*, *86*, 7210–7254.

Lowe, D. C., and U. Schmidt (1983), Formaldehyde (HCHO) measurements in the nonurban atmosphere, *J. Geophy. Res.*, *88*, 10,844–10,858.

Lurmann, F. W., A. C. Lloyd, and R. Atkinson (1986), A chemical mechanism for use in long-range transport/acid deposition computer modeling, *J. Geophys. Res.*, *91*, 10,905–10,936.

Mauldin, R. L., III, G. J. Frost, G. Chen, D. J. Tanner, A. S. H. Prevot, D. D. Davis, and F. L. Eisele (1998), OH measurements during the first aerosol characterization experiment (ACE 1), Observations and model comparisons, *J. Geophys. Res.*, *103*, 16,713–16,729.

Mauldin, R. L., III, D. J. Tanner, and F. L. Eisele (1999), Measurements of OH during PEM Tropics, *J. Geophys. Res.*, *104*, 5817–5827.

Mauldin, R., et al. (2003), Highlights of OH, H_2SO_4 and MSA measurements made aboard the NASA P-3B during TRACE-P, *J. Geophys. Res.*, *108*(D20), 8796, doi:10.1029/2003JD003410.

McKeen, S. A., T. Gierczak, J. B. Burkholder, P. O. Wennberg, T. F. Hanisco, E. R. Keim, R.-S. Gao, S. C. Liu, A. R. Ravishankara, and D. W. Fahey (1997), The photochemistry of acetone in the upper troposphere: A source of odd-hydrogen radicals, *Geophys. Res. Lett.*, *24*, 3177–3180.

Olson, J., et al. (2001), Seasonal differences in the photochemistry of the South Pacific: A comparison of observations and model results from PEM-Tropics A and B, *J. Geophys. Res.*, *106*, 32,749–32,766.

Prather, M. J., and D. J. Jacob (1997), A persistent imbalance in HO_x and NO_x photochemistry of the upper troposphere driven by deep tropical convection, *Geophys. Res. Lett.*, *24*, 3189–3192.

Ravishankara, A. R., E. J. Dunlean, M. A. Blitz, T. J. Dillon, D. E. Heard, M. J. Pilling, R. S. Strekowski, J. M. Nicovich, and P. H. Wine (2002), Redetermination of the rate coefficient for the reaction of O (^1D) with N_2, *Geophys. Res. Lett.*, *29*(15), 1745, doi:10.1029/2002GL014850.

Roehl, C. A., S. A. Nizkorodov, G. A. Blake, and P. O. Wennberg (2002), Photodissociation of peroxynitric acid in the near IR, *J. Phys. Chem. A.*, *106*(15), 3766–3772.

Salawitch, R. J., P. O. Wennberg, G. C. Toon, B. Sen, and J.-F. Blavier (2002), Near IR photolysis of HO_2NO_2: Implications for HO_x, *Geophys. Res. Lett.*, *29*(16), 1762, doi:10.1029/2002GL015006.

Sander, S. P., et al. (2000), Chemical kinetics and photochemical data for use in stratospheric modeling: Supplement to Evaluation 12: Update of key reactions, *JPL Publ.*, *00–3*.

Shetter, R. E., and M. Müller (1999), Photolysis frequency measurements using actinic flux spectroradiometery during the PEM-Tropics mission: Instrumentation description and some results, *J. Geophys. Res.*, *104*, 5647–5661.

Sigsby, J. E., S. Gejada, W. Ray, J. M. Lang, and J. W. Duncan (1987), Volatile organic compound emissions from 46 in-use passenger cars, *Environ. Sci. Technol.*, *21*, 466–475.

Singh, H. B., M. Kanakidou, P. J. Crutzen, and D. J. Jacob (1995), High concentrations and photochemical fate of oxygenated hydrocarbons in the global troposphere, *Nature*, *378*, 50–54.

TRACE-P Science Team (2003), Preface to the NASA Global Tropospheric Experiment Transport and Chemical Evolution Over the Pacific (TRACE-P): Measurements and analysis, *J. Geophys. Res.*, *108*(D20), 8780, doi:10.1029/2003JD003851.

Wagner, V., R. von Glascow, H. Fischer, and P. J. Crutzen (2002), Are CH_2O measurements in the marine boundary layer suitable for testing the current understanding of CH_4 photooxidation?, *J. Geophys. Res.*, *107*(D3), 4029, doi:10.1029/2001JD000722.

Wang, Y., et al. (2002), Springtime photochemistry at northern mid and high latitudes, *J. Geophys. Res.*, *108*(D4), 8358, doi:10.1029/2002JD002227.

Weller, R. O., O. Schrems, A. Boddenberg, S. Gäb, and M. Gautrois (2000), Meridional distribution of hydroperoxides and formaldehyde in the marine boundary layer of the Atlantic (48°N–25°S) measured during the Albatross campaign, *J. Geophys. Res.*, *105*, 14,401–14,412.

Wennberg, P. O., et al. (1998), Hydrogen radicals, nitrogen radicals, and the production of O_3 in the upper troposphere, *Science*, *279*, 49–53.

Wennberg, P. O., et al. (1999), Twilight observations suggest unknown sources of HO_x, *Geophys. Res. Lett.*, *26*, 1373–1376.

Zhou, X., Y.-N. Lee, L. Newman, X. Chen, and K. Mopper (1996), Tropospheric formaldehyde concentration at the Mauna Loa Observatory during the Mauna Loa Observatory Photochemistry Experiment 2, *J. Geophys. Res.*, *101*, 14711–14719.

B. E. Anderson, M. A. Avery, J. D. Barrick, G. Chen, J. H. Crawford, C. E. Jordan, J. R. Olson, and G. W. Sachse, Atmospheric Sciences Division, Langley Research Center, NASA, Hampton, VA 23681, USA. (b.e.anderson@larc.nasa.gov; m.a.avery@larc.nasa.gov; j.d.barrick@larc.nasa.gov; g.chen@larc.nasa.gov; james.h.crawford@nasa.gov; c.e.jordan@larc.nasa.gov; j.r.olson@larc.nasa.gov; g.w.sachse@larc.nasa.gov)

D. R. Blake, Department of Chemistry, University of California, 516 Rowland Hall, Irvine, CA 92697-2025, USA. (drblake@uci.edu)

W. H. Brune, Department of Meteorology, Pennsylvania State University, 503 Walker Building, University Park, PA 16802, USA. (brune@essc.psu.edu)

D. D. Davis, S. T. Sandholm, and D. Tan, School of Earth and Atmospheric Sciences, Georgia Institute of Technology, Baker Bldg., Room 107, Atlanta, GA 30332, USA. (douglas.davis@eas.gatech.edu; scott.sandholm@eas.gatech.edu; dtan@eas.gatech.edu)

F. L. Eisele, F. Flocke, A. Fried, B. L. Lefer, R. L. Mauldin, and R. E. Shetter, Atmospheric Chemistry Division, NCAR, 1850 Table Mesa Drive, Boulder, CO 80303, USA. (eisele@ncar.ucar.edu; ffl@acd.ucar.edu; fried@acd.ucar.edu; lefer@ucar.edu; mauldin@ucar.edu; shetter@ucar.edu)

M. J. Evans and D. J. Jacob, Division of Engineering and Applied Science, Harvard University, 29 Oxford Street, Cambridge, MA 02138, USA. (mje@io.harvard.edu; djj@io.harvard.edu)

H. Harder and M. Martinez, Max Planck Institute for Chemistry, J.J. Becherweg 27, D-55128 Mainz, Germany. (harder@mpch-mainz.mpg.de; martinez@mpch-mainz.mpg.de)

Y. Kondo, Solar-Terrestrial Environmental Laboratory, Nagoya University, 3-13 Honohara, Toyokawa, Aichi 422-8507, Japan. (kondo@stelab.nagoya-u.ac.jp)

H. B. Singh, NASA Ames Research Center, Mail Stop 245-5, Moffett Field, CA 94035, USA. (hanwant.b.singh@nasa.gov)

R. W. Talbot, EOS, CCRC, Morse Hall, University of New Hampshire, Durham, NH 03824, USA. (robert.talbot@unh.edu)